Thermal Diffuse Scattering as a Probe of Large-Wave-Vector Phonons in Silicon Nanostructures

Gokul Gopalakrishnan, Martin V. Holt, Kyle M. McElhinny, Josef W. Spalenka, David A. Czaplewski, Tobias U. Schülli, and Paul G. Evans

Phys. Rev. Lett. **110**, 205503 — Published 14 May 2013

DOI: 10.1103/PhysRevLett.110.205503

Thermal Diffuse Scattering as a Probe of Large-Wavevector Phonons in Silicon Nanostructures

Gokul Gopalakrishnan,[1a)] Martin V. Holt,[2] Kyle M. McElhinny,[1] Josef W. Spalenka,[1] David A. Czaplewski,[2] Tobias U. Schülli,[3] and Paul G. Evans[1b)]

[1] Materials Science and Engineering and Materials Science Program, University of Wisconsin, Madison, WI 53706, USA

[2] Center for Nanoscale Materials, Argonne National Laboratory, Argonne, IL 60439, USA

[3] European Synchrotron Radiation Facility, F-38043 Grenoble, France

Large-wavevector phonons have an important role in determining the thermal and electronic properties of nanoscale materials. The small volumes of such structures, however, have posed significant challenges to experimental studies of the phonon dispersion. We show that synchrotron x-ray thermal diffuse scattering (TDS) can be adapted to probe phonons with wavevectors spanning the entire Brillouin zone of nanoscale silicon membranes. The TDS signal from flat Si nanomembranes with thicknesses from 315 nm to 6 nm, and a sample volume as small as 5 μm^3, has the expected linear dependence on the membrane thickness and also exhibits excess intensity at large wavevectors, consistent with the scattering signature expected from low-lying large-wavevector modes of the membranes.

[a)] Electronic mail: gokul@engr.wisc.edu.

[b)] Electronic mail: evans@engr.wisc.edu.

Materials design and discovery at the nanoscale is driven by the opportunity to modify the fundamental excitations of solids by reducing the size of crystals, and introducing engineered boundary conditions. The connection between phonons, the fundamental quanta of vibrational excitations, and mechanical, optical, electronic and thermal properties has been rigorously established in extended solids. An analogous connection is beginning to be exploited in the discovery of novel thermal transport phenomena in nanomaterials ranging from inorganic semiconductors [1] to graphene [2], with greater opportunity for innovation than in bulk systems of the same chemical compositions [3, 4]. These efforts face the fundamental challenge that experimental insight into the full phonon dispersion of nanomaterials has not been available.

Large-wavevector phonons have an important role in the properties of two-dimensional silicon nanomaterials [5]. The thermal conductivity and thermoelectric figure of merit of Si sheets with nanoscale thicknesses differ significantly from their bulk values [4, 6-8]. In addition, electronic transport in Si involves the scattering of electrons between conduction band valleys by large-wavevector phonons [9], a process which is in turn influenced by varying the size of the crystal [10, 11]. Because of these effects, the importance of the phonon dispersion in Si and related nanomaterials has long been recognized, leading to repeated experimental efforts to study phonons in nanoscale volumes [12-14].

Elasticity theory describes the vibrational modes of thin elastic membranes in a continuum approximation [15, 16]. The solutions provided by elasticity theory have been used to obtain the atomic displacements and frequencies associated with low-wavevector phonons in semiconductor nanostructures [4, 17]. In thin sheets, the periodic boundary conditions applicable to extended solids are replaced by vanishing normal components of the stress at the free surfaces, yielding four modes of vibration that are not found in the bulk: two shear modes (symmetric and

antisymmetric), a flexural mode, and a dilatational mode. The flexural and dilatational modes have mixed transverse and longitudinal acoustic character, and are particularly interesting because both can have phonon frequencies lower than the normal modes of the bulk crystal. In the limit where the membrane thickness far exceeds the characteristic coherence lengths of phonons, these modes evolve into a pair of Rayleigh waves localized near each surface.

At present, experimental and theoretical studies of the phonon dispersion of nanowires and sheets are primarily restricted to high-energy optical phonons and to acoustic phonons at momenta near the center of the Brillouin zone, with wavevectors smaller than 0.1 $2\pi/a$, where a is the Si lattice parameter [18-20]. At these wavevectors, the vibrational properties of nanomembranes have been widely probed by optical techniques, such as Raman and Brillouin scattering [14, 21-23]. Phonon dispersions in macroscopic samples and in macroscopic quantities of zero-dimensional nanostructures have been probed by inelastic x-ray or neutron scattering [24-27]. Energy-resolved inelastic scattering techniques require samples with volumes of 10^3 μm^3 or more. One can overcome this problem in specific cases: for instance, the lattice vibrations of zero-dimensional nanostructures (i.e. nanoparticles and quantum dots) lack a dispersion, and can be probed in large ensembles, as their relative orientations are unimportant [28]. In one- and two-dimensional nanostructures it is challenging to create sufficient volumes of well-aligned ensembles to match the sensitivity of energy-resolved inelastic neutron or x-ray techniques.

X-ray thermal diffuse scattering (TDS) is an energy-integrated analog of inelastic scattering that provides the capability to simultaneously probe phonons across the entire Brillouin zone, with high momentum resolution. The intensity distribution recorded in TDS measurements is determined by the dispersion and polarization of thermally populated phonon modes [29]. The first-order TDS intensity at wavevector **S** in reciprocal space, as shown in Fig. 1(a), is

determined by phonons with wavevector **Q**, where **Q** is the difference between **S** and the nearest point **G** on the reciprocal lattice [29]. X-ray TDS is highly sensitive to small changes in the frequency of the lowest lying acoustic phonon modes at wavevectors far from Bragg reflections due to an approximately $1/\omega^2$ dependence of the intensity at low values of the phonon frequency ω, and a lack of competing elastic scattering processes at these conditions [30]. In this Letter, we show that synchrotron x-ray TDS reveals key features of the acoustic phonon dispersion in Si nanomembranes over a wide range of wavevectors extending from the Brillouin zone center to the zone boundaries. We demonstrate that this technique can be used to probe large wavevector phonons in nanoscale ensembles with volumes as small as 4 μm^3.

Silicon membranes with thicknesses ranging from 6 to 315 nm were fabricated from ultrathin silicon-on-insulator (SOI) wafers [31]. Improved fabrication techniques yield flat unbuckled membranes, as shown in Fig. 1(b), which make it possible to measure the TDS signal free from spurious effects from the static strain field. In addition, advances in synchrotron radiation instrumentation, including the development of highly stable nanofocusing beamlines have enabled the detection of low-intensity TDS signals from the small volume of material in nanomembranes. TDS experiments were performed at room temperature at station 26-ID-C of the Advanced Photon Source at Argonne National Laboratory. The measurements were conducted in vacuum using a transmission geometry with the incident x-ray beam along the surface normal of the nanomembrane. A beam of 10 keV x-ray photons, focused by a capillary condenser, illuminated a 30 μm-diameter region of the membrane. A charge-coupled device recorded the intensity of x-rays scattered to a two-dimensional section of reciprocal space near the (1 3 -1) reciprocal lattice point. As shown in Fig. 1(a), the area spanned by the x-ray detector

corresponds to a curved surface in reciprocal space that passes near the Γ-point at the zone center and intersects the Brillouin zone boundary near the X symmetry point.

Three sets of measurements were performed to acquire TDS intensity distributions: (i) a measurement of the TDS intensity from the Si membrane with the x-ray beam directed through the center of the suspended membrane, (ii) a bulk measurement with the beam passing through a thickness of approximately 100 μm of the SOI handle wafer, and (iii) a background measurement with the beam passing through an open window. Open windows were created by mechanically removing a membrane. Each series of measurements involved several consecutive repetitions of a pair of exposures that were double-correlated to eliminate random events. An averaged background image was subtracted from the averaged membrane or bulk image to remove contributions to the detected x-ray intensity arising from sources outside the sample.

The distribution of TDS intensity for a 315 nm-thick membrane is shown in Fig. 1(c). The region of high TDS intensity near the center of the Brillouin zone arises from the large thermal population of low-energy acoustic phonons. The isolated sharp bright spot to the left of the maximum in the TDS intensity results from the intersection of the Si crystal truncation rod, shown schematically in Fig. 1(a), with the reciprocal space sheet spanned by the detector. The intersection of the Ewald sphere with boundaries of the Brillouin zone centered on the (1 3 -1) reciprocal lattice point is overlaid on the detector image.

A diagonal streak of intensity extends from near the zone center in Fig. 1(c) towards the vicinity of the X-point on the zone boundary. The TDS intensity is expected to be high along this path, even in bulk crystals, due to the elastic anisotropy of Si [29]. The quantity Q_x indicated in Fig. 1(c) is the projection of the phonon wave vector onto the [1 0 0] direction, the x axis of reciprocal space. Values of Q_y and Q_z along this streak are smaller than 0.25 $2\pi/a$, and do not

vary significantly along the direction of the high-intensity streak. The bulk Si phonon dispersion [32] along the [1 0 0] direction is shown in Fig. 1(d). The low-energy doubly degenerate transverse acoustic (TA) branches are particularly important as they contribute approximately 90% of the total TDS intensity along this direction. The low-frequency modes of nanomembranes have frequencies below the bulk TA modes [4], as illustrated in Fig. 1(e), and have large atomic displacements near the surface of the membrane, as shown in Fig. 1(f).

The experimentally observed bulk TDS intensity distribution and the first-order TDS predicted using the bulk phonon dispersion [33] are shown in Figs. 2(a) and 2(b). Multiplying the predicted intensity by a single scaling parameter results in excellent agreement with the measured intensity [29,33]. Figure 2(c) shows the predicted and observed bulk intensities along the indicated paths on the detector, from the intensity maximum of the TDS near the zone center to the zone boundary.

The variation of TDS intensity as a function of the thickness of the Si nanomembrane is shown in Figs. 3(a) and 3(b). The variation is shown for representative points in reciprocal space: one near the zone center, and the other on the zone boundary, with $Q_x=2\pi/a$. Sample-to-sample variation in the small-thickness regime arises in part from small deviations in the orientation arising from the sample mounting procedure. Intensity distributions for Si nanomembranes with thicknesses of 315, 44, 28 and 6 nm are shown in Figs. 3(c)-(f). Membranes with reduced thicknesses have lower TDS intensity and a relative increase in the intensity of the Si truncation rod. For thick membranes (e.g. 315 nm), the TDS intensity distribution closely matches the intensity arising from bulk with the notable exception of a small excess intensity at wavevectors approaching $2\pi/a$. These deviations become more apparent in thinner membranes (e.g. 44 nm and 28 nm). In the thinnest membranes (e.g. 6 nm), the weak TDS signal at the largest

wavevectors coincides with a large contribution to the intensity from residual background scattering and static scattering from the oxide at the membrane surface.

The difference between TDS from nanoscale sheets and bulk thicknesses is apparent in the dependence of the TDS intensity on the wavevector Q_x. The dependence of the membrane TDS intensity on Q_x is shown in Figs. 4(a)-(d) (black dots). The reciprocal-space paths for Fig. 4 follow the high intensity streak close to the Γ-X direction, similar to the path chosen for the bulk sample shown in Fig. 2(a). Figure 4 compares the nanomembrane TDS intensity with the intensity measured along the same reciprocal space paths using the bulk SOI support of each membrane. The membrane and bulk profiles are each normalized to unity at their peak intensity of 1, and offset in Fig. 4 for clarity. A broad excess in the TDS intensity at wave vectors between approximately 3/2 π/a and 2 π/a along the high intensity streak emerges in membranes with small thicknesses.

A confinement-induced reduction in the phonon energy by as little as 1 meV would be sufficient to yield an increase of 10% in TDS intensity for wavevectors near the Brillouin zone boundary. Previously, confinement energies on the order of 0.5 meV in 30-nm-thick membranes have been established in the low-wavevector regime [21]. The intensity deviations we observe here at similar thicknesses are consistent with the energy scale of these previous results, but occur at larger wavevectors at which different modes of vibration are relevant. Elasticity calculations, as in Figs. 1(e) and 1(f), employ a continuum elastic approximation and are therefore limited to long-wavelength modes for which the length-scale imposed by atomic bonding is irrelevant. A more detailed comparison of the experimental results with theory will require the computation of phonon dispersions based on atomistic rather than continuum theories. Such predictions yield similar large-surface-displacement vibrational modes with very

low frequencies in Si nanowires [34], but are not yet available for Si membranes with thicknesses of many nanometers.

Synchrotron x-ray TDS allows the experimental study and engineering of phonons in nanostructures to move beyond approximations that are valid only in the low-wavevector regime [9], and can contribute to an expanded toolbox for the design of novel thermal and electronic devices. The deviations from bulk TDS intensities observed here at large wavevectors suggest that the dispersion of large-wavevector phonons in silicon membranes with thicknesses in the tens of nanometers and smaller is substantially different than in bulk Si. Phonons in this regime are thermally relevant in silicon nanostructures because the longer-wavelength small-wavevector phonons are efficiently scattered at boundaries and contribute less to thermal conduction at the nanoscale [6]. Similar modes are also electronically relevant to the intervalley-scattering-limited electron mobility of lightly doped silicon [35]. In addition to the Si materials system, TDS can allow large-wavevector acoustic phonons to be probed at the nanoscale in systems where phonons determine phase transformations and thermal transport phenomena, and for which experimental insight has been available only in bulk-scale samples [36-38]. Further advances in x-ray nanobeam techniques will allow TDS studies to be conducted on individual nanostructures in these emerging materials via the creation of tightly focused, highly intense x-ray beams [39].

GG, KM, and PE acknowledge support from the US Air Force Office of Scientific Research, through contract FA9550-10-1-0249, and support from the European Synchrotron Radiation Facility for initial synchrotron radiation measurements. JS acknowledges support from the University of Wisconsin Materials Research Science and Engineering Center, NSF grant no. DMR-1121288. MH and DC, as part of the Center for Nanoscale Materials core research

program, and use of the Advanced Photon Source were supported by the U. S. Department of Energy, Office of Science, Office of Basic Energy Sciences, under Contract No. DE-AC02-06CH11357. The authors gratefully acknowledge Dr. Ralu Divan, at the Center for Nanoscale Materials, and Dr. Rob Ilic, at the Cornell Nanoscale Science and Technology Facility, for assistance with the fabrication of silicon membranes.

Figure 1 (a) First-order thermal diffuse scattering with a momentum transfer **S** arises from phonons with wave vector **Q**. **G** is the reciprocal lattice vector closest to **S**. Bragg reflections from silicon membranes are elongated into rods of intensity along the direction normal to the surface of the membrane. The reciprocal-space representation of the x-ray detector (curved blue surface) passes near the zone center and intersects the boundary of the Brillouin zone centered on the (1 3 -1) reciprocal lattice point (orange polyhedron). (b) Optical micrograph of a flat silicon membrane with a thickness of 315 nm. (c) TDS intensity distribution from a membrane with a thickness of 315 nm. Boundaries of Brillouin zones are shown as orange lines. (d) Bulk phonon dispersion for Si along the [1 0 0] direction, with transverse acoustic (TA), longitudinal acoustic (LA), transverse optical (TO) and longitudinal optical (LO) branches. (e) Dispersions of the lowest flexural (LFM) and dilatational (LDM) modes of a 10-nm-thick silicon membrane, after ref. [4], compared with bulk acoustic modes. The energy-wavevector regime of the comparison is indicated by the red rectangle in the bulk dispersion. (f) Directions and relative magnitudes of near-surface atomic displacements in a Si nanomembrane for an example of the lowest-frequency dilatational mode.

Figure 2 (a) Experimentally observed TDS intensity for a bulk-like thickness of the SOI handle wafer. (b) Predicted first-order TDS intensity based on the bulk phonon dispersion. (c) Intensity profile of the measured TDS intensity (points) and TDS predicted from the bulk Si phonon dispersion (line) along the paths indicated in (a) and (b).

Figure 3 Variation of nanomembrane TDS within reciprocal space regions (a) near the zone center and (b) at the zone edge, near the X-point. Intensities were corrected for exposure time and incident flux. The dashed line is a fit through to guide the eye. (c)-(f) Nanomembrane thermal diffuse scattering intensity distributions for membranes with thicknesses of 315 nm, 44

nm, 28 nm and 6 nm, normalized to the TDS intensity maximum in each image. The bright spot to the left of the maximum in the diffuse scattering arises from the crystal truncation rod. Orange lines represent zone boundaries.

Figure 4 Dependence of the TDS intensity on the wavevector Q_x for (a) 315 nm, (b) 44 nm, (c) 28 nm, and (d) 6 nm membranes (black circles) and for bulk-like regions of the SOI handle wafer for each sample (red squares). The intensity profiles are normalized to unity at their maxima and offset vertically for clarity. The central maximum in (d) is sharper than in thicker samples due to a small difference in the sample orientation.

Gopalakrishnan *et al*., Figure 1

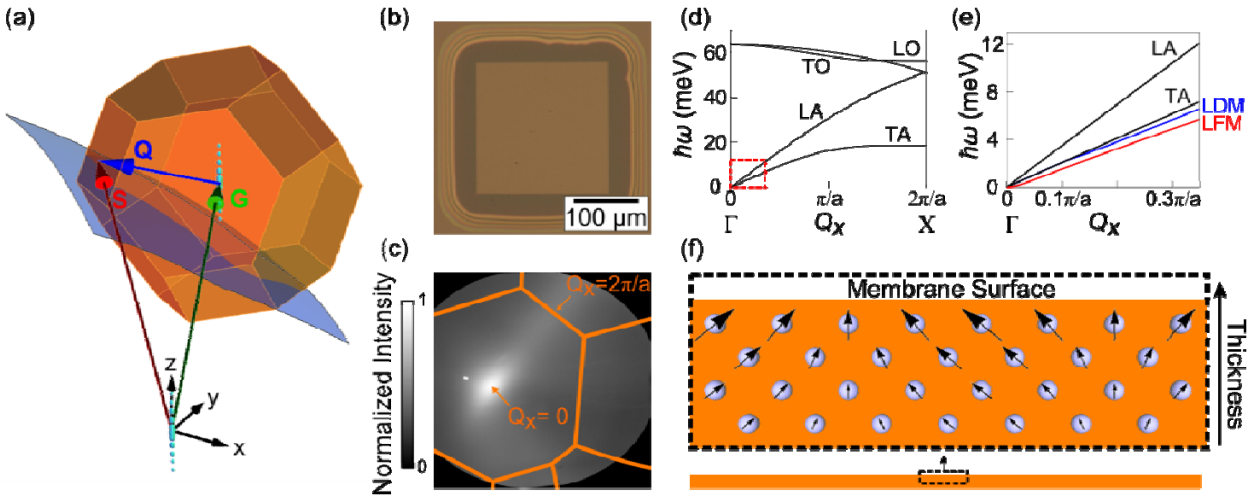

Gopalakrishnan *et al*., Figure 2

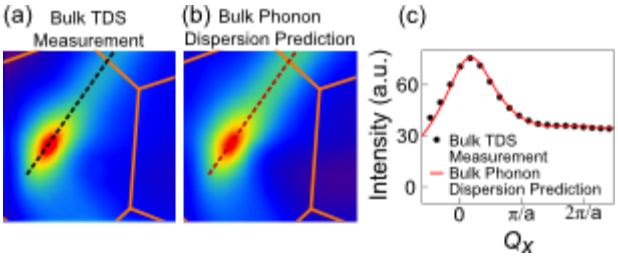

Gopalakrishnan *et al*., Figure 3

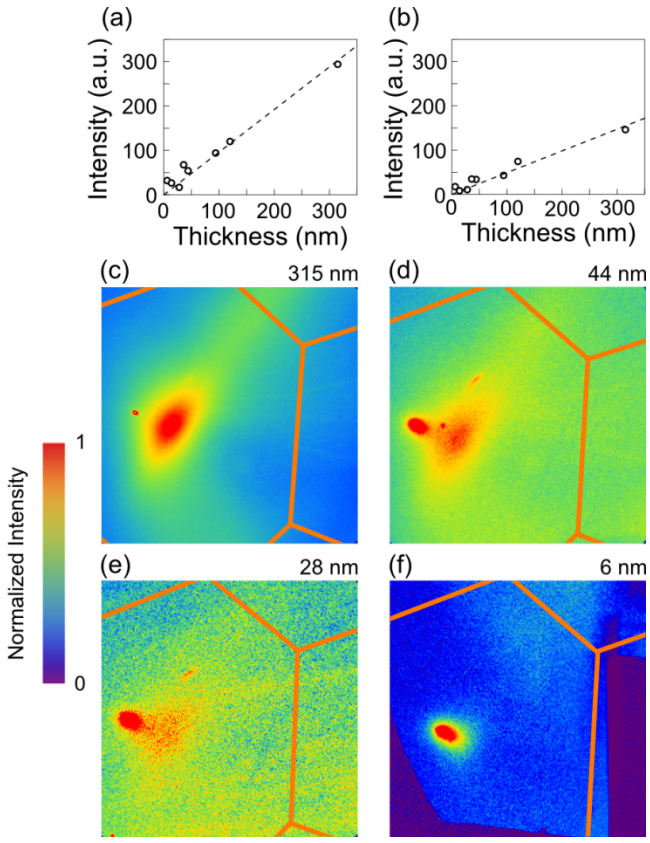

Gopalakrishnan *et al*., Figure 4

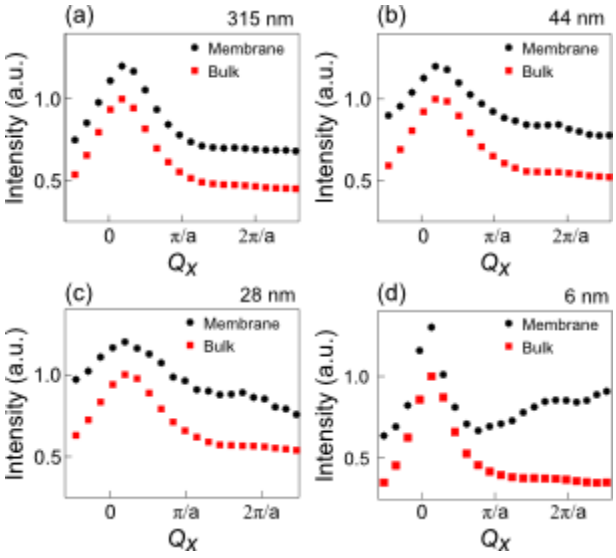

[1] P. F. R. Poudeu, J. D'Angelo, A. D. Downey, J. L. Short, T. P. Hogan, and M. G. Kanatzidis, Angew. Chemie-Int. Ed. **45**, 3835 (2006).

[2] S. Chen, Q. Wu, C. Mishra, J. Kang, H. Zhang, K. Cho, W. Cai, A. A. Balandin, and R. S. Ruoff, Nat. Mater. **11**, 203 (2012).

[3] D. G. Cahill, W. K. Ford, K. E. Goodson, G. D. Mahan, A. Majumdar, H. J. Maris, R. Merlin, and S. R. Phillpot, J. Appl. Phys. **93**, 793 (2003).

[4] A. Balandin and K. L. Wang, Phys. Rev. B **58**, 1544 (1998).

[5] J. A. Rogers, M. G. Lagally, and R. G. Nuzzo, Nature **477**, 45 (2011).

[6] Y. S. Ju, and K. E. Goodson, Appl. Phys. Lett. **74**, 3005 (1999).

[7] W. J. Liu and M. Asheghi, J. Heat Transf. - Trans. ASME **128**, 75 (2006).

[8] A. Balandin and K. L. Wang, J. Appl. Phys. **84**, 6149 (1998).

[9] C. Jacoboni and L. Reggiani, Rev. Mod. Phys. **55**, 645 (1983).

[10] E. Pop, R. W. Dutton, and K. E. Goodson, J. Appl. Phys. **96**, 4998 (2004).

[11] M. J. Gilbert, R. Akis, and D. K. Ferry, J. Appl. Phys. **98**, 094303 (2005).

[12] H. Reichert, F. Bencivenga, B. Wehinger, M. Krisch, F. Sette, and H. Dosch, Phys. Rev. Lett. **98**, 096104 (2007).

[13] R. L. Dennis, and M. B. Webb, J. Vac. Sci. Technol. **10**, 192 (1973).

[14] J. Cuffe, E. Chavez, A. Shchepetov, P.-O. Chapuis, E. H. El Boudouti, F. Alzina, T. Kehoe, J. Gomis-Bresco, D. Dudek, Y. Pennec, B. Djafari-Rouhani, M. Prunnila, J. Ahopelto, and C. M. Sotomayor Torres, Nano Lett. **12**, 3569 (2012).

[15] H. Lamb, Proc. Roy. Soc. A **93**, 114 (1917).

[16] R. D. Mindlin and M. A. Medick, J. Appl. Mech. **26**, 561 (1959).

[17] N. Bannov, V. Aristov, V. Mitin, and M. A. Stroscio, Phys. Rev. B **51**, 9930 (1995).

[18] K. W. Adu, Q. Xiong, H. R. Gutierrez, G. Chen, and P. C. Eklund, Appl. Phys. A **85**, 287 (2006).

[19] J. F. Qi, J. M. White, A. M. Belcher, and Y. Masumoto, Chem. Phys. Lett. **372**, 763 (2003).

[20] K. W. Adu, H. R. Gutierrez, U. J. Kim, G. U. Sumanasekera, and P. C. Eklund, Nano Lett. **5**, 409 (2005).

[21] J. Groenen, F. Poinsotte, A. Zwick, C. M. Sotomayor Torres, M. Prunnila, and J. Ahopelto, Phys. Rev. B **77**, 045420 (2008).

[22] C. M. Sotomayor Torres, A. Zwick, F. Poinsotte, J. Groenen, M. Prunnila, J. Ahopelto, A. Mlayah, and V. Paillard, Phys. Status Solidi C **1**, 2609 (2004).

[23] R. S. Bandhu, R. Sooryakumar, and K. Bussmann, Ann. Phys.-Berlin **523,** 107 (2011).

[24] G. Nilsson and G. Nelin, Phys. Rev. B **6**, 3777 (1972).

[25] M. Schwoerer-Bohning, A. T. Macrander, and D. A. Arms, Phys. Rev. Lett. **80**, 5572 (1998).

[26] L. Saviot, C. H. Netting, D. B. Murray, S. Rols, A. Mermet, A.-L. Papa, C. Pighini, D. Aymes, and N. Millot, Phys. Rev. B **78**, 245426 (2008).

[27] O. Delaire, J. Ma, K. Marty, A. F. May, M. A. McGuire, M. H. Du, D. J. Singh, A. Podlesnyak, G. Ehlers, M. D. Lumsden, and B. C. Sales, Nature Mater. **10**, 614 (2011).

[28] U. Stuhr, H. Wipf, K. H. Andersen, and H. Hahn, Phys. Rev. Lett. **81**, 1449 (1998).

[29] M. Holt, Z. Wu, H. W. Hong, P. Zschack, P. Jemian, J. Tischler, H. Chen, and T. C. Chiang, Phys. Rev. Lett. **83**, 3317 (1999).

[30] M. Holt, P. Zschack, H. Hong, M. Y. Chou, and T. C. Chiang, Phys. Rev. Lett. **86**, 3799 (2001).

[31] G. Gopalakrishnan, D. A. Czaplewski, K. M. McElhinny, M. V. Holt, J. C. Silva-Martinez, and P. G. Evans, Appl. Phys. Lett. **102**, 033113 (2013).

[32] R. Tubino, G. Zerbi, and L. Piseri, J. Chem. Phys. **56**, 1022 (1972).

[33] See Supplemental Material at [ ] for calculation of bulk TDS intensities and comparison with measured TDS intensity patterns.

[34] T. Thonhauser and G. D. Mahan, Phys. Rev. B **69**, 075213 (2004).

[35] F. Murphy-Armando, G. Fagas, and J. C. Greer, Nano Lett. **10**, 869 (2010).

[36] A. A. Sirenko, C. Bernhard, A. Golnik, A. M. Clark, J. H. Hao, W. D. Si, and X. X. Xi, Nature **404**, 373 (2000).

[37] J. Wu, Q. Gu, B. S. Guiton, N. P. de Leon, O. Lian, and H. Park, Nano Lett. **6**, 2313 (2006).

[38] M. Christensen, A. B. Abrahamsen, N. B. Christensen, F. Juranyi, N. H. Andersen, K. Lefmann, J. Andreasson, C. R. H. Bahl, and B. B. Iversen, Nat. Mater. **7,** 811 (2008).

[39] G. E. Ice, J. D. Budai, and J. W. L. Pang, Science **334**, 1234 (2011).